



Aggregation of casein micelles induced by Ca²⁺ during in vitro digestion: Effects on the release of loaded anthocyanins

Journal:	<i>Food & Function</i>
Manuscript ID	FO-ART-08-2023-003684.R2
Article Type:	Paper
Date Submitted by the Author:	03-Dec-2023
Complete List of Authors:	Ren, Jinbo; China Agricultural University Liao, Minjie; China Agricultural University Li, Kaixin; China Agricultural University Chen, Fang; China Agricultural University Hu, Xiaosong; China Agricultural University Ma, Lingjun; China Agricultural University Ji, Junfu; China Agricultural University

ARTICLE

Aggregation of casein micelles induced by Ca²⁺ during *in vitro* digestion: Effects on the release of loaded anthocyanins†

Jinbo Ren,^{a,b} Minjie Liao,^a Kaixin Li,^a Fang Chen,^a Xiaosong Hu,^{a,b} Lingjun Ma,^{*a,b} Junfu Ji,^{*a,b}

Received 00th January 20xx,
Accepted 00th January 20xx

DOI: 10.1039/x0xx00000x

Colloidal calcium phosphate (CCP) confers a modifiable structure to micellar casein (MC), which provides it with potential advantages as a delivery carrier. However, it is difficult to achieve multi-pattern release of the core material in intestine with MC as a single wall. In this study, we prepared an anthocyanin-casein delivery system utilizing MC with different freezing degrees as the wall material with the objective of achieving controlled release of model core anthocyanin in intestine. The results showed that freezing could significantly reduce the CCP level up to 50%. Static *in vitro* simulated digestion with adding exogenous Ca²⁺ showed that the designed delivery system exhibited low anthocyanin release (15–35%) in gastric tract. The pattern of release in intestine depended on CCP dissociation degree. High and low dissociation degrees corresponded to slow release (from 15% to 65% within 2 h) and burst release (from 35% to 90% within 5 min), respectively. WAXS/SAXS analysis revealed that exogenous serum Ca²⁺ inherent in simulated gastric fluid and endogenous serum Ca²⁺ induced by CCP dissociation were synergistically involved in reconstitution of CCP-mediated nanoclusters and large aggregates. The freezing degree of MC determined the endogenous serum Ca²⁺ level, which influenced the gastric aggregation behavior of wall MC and ultimately led to a quite different gastrointestinal release behavior of anthocyanins.

1 Introduction

In studies related to oral drug delivery, the stomach and small intestine are the main sites of digestion and absorption, respectively.^{1,2} It means that structural changes of wall material in stomach significantly affect the release pattern of the loaded core material in small intestine.³ When it comes to specific diseases and a 'top-down' view of carriers must be constructed, i.e., the slow or burst release of the core material in small intestine has been confirmed⁴, which highlights the necessity of a specific design for wall materials.

Natural micellar casein (MC) has a relatively open and flexible conformation, consisting of casein subunits ($\alpha_s/\beta/\kappa$ -casein) linked mainly by colloidal calcium phosphate (CCP) and hydrophobic interactions.⁵ Current studies on the delivery of functional components using MC as a wall material excessively rely on the complex construction for adequate intestinal controlled release purposes.^{6–10} It inevitably leads to the introduction of chemical reagents (e.g., for pH adjustment and cross-linking), which pose an obstacle to the availability of the core as a daily nutritional supplement. It is difficult to achieve multi-modal release of the core material in intestine with MC as a single wall material. It reminds us to take full advantage of the

flexible and adjustable structure of MC and to deepen our insight into structural changes of casein micelles in gastrointestinal tract. Studies have shown that κ -casein cleaved by pepsin on MC surface exposes the internal CCP-mediated nanoclusters and expands further into large aggregates via Ca²⁺ cross-linking.^{11,12} The increasing aggregation behavior is controlled by CCP level, and the subsequent digestion behavior is also dominated by it.¹³ Therefore, it seems essential to regulate CCP level in micelle structure.

A dynamic equilibrium system consisting of colloidal phase and serum phase exists in casein micelle.¹⁴ CCP is abundantly present in the colloidal phase. Low temperature environment contributes to releasing part of Ca²⁺ from colloidal phase to serum phase, which results in CCP dissociation.¹⁵ However, the interphase transition induced by low temperature is temporary. Because dissociated CCP can be rapidly reconstituted in solution once the temperature is increased.¹⁶ In our previous work¹⁷, MC was treated to different freezing levels by controlling the droplet size of spray freeze drying (SFD), thus obtaining SFD powders with different CCP levels. SFD powders exhibited excellent rehydration performance in deionized water due to the partial absence of CCP. However, it does not indicate that the core material must be released in the burst pattern. As the complex environment of the stomach involving pepsin, gastric acid and serum Ca²⁺ can modify the micelle structure^{18,19}, which might subsequently influence the release pattern of the core material in small intestine.

Anthocyanins (ACNs) are water-soluble pigments containing 2-phenylchroman moieties, which are absorbed in small intestine about 10%–25%.²⁰ Its chemical structure contains reactive oxygen and hydroxyl groups and hence normally

^a College of Food Science and Nutritional Engineering, National Engineering Research Center for Fruit and Vegetable Processing, China Agricultural University, Key Lab of Fruit and Vegetable Processing, Ministry of Agriculture and Rural Affairs, Beijing 100083, China.

^b Xinghua Industrial Research Centre for Food Science and Human Health, China Agricultural University, Xinghua 225700, China.

E-mail: lingjun.ma@cau.edu.cn; junfu.ji@cau.edu.cn

† Electronic Supplementary Information (ESI) available. See DOI: <https://doi.org/10.1039/x0xx00000x>

exhibits poor stability.²¹ Enzymes, salt ions and pH in gastrointestinal tract lead to degradation and discoloration of ACNs.^{22,23} In this study, ACNs were selected as model cores loaded in MC with different CCP levels controlled by SFD. Spray-dried and freeze-dried powdery samples of relatively intact CCP were prepared as controls. Then, *in vitro* simulated digestion experiments with and without adding exogenous serum Ca²⁺ were performed. Dissolution and hydrolysis degrees of ACNs-MC powders during digestion and serum Ca²⁺ level in digesta were investigated. Furthermore, the precise structure of the aggregates obtained from the digesta was characterized by wide-angle combined small-angle X-ray scattering (WAXS/SAXS). The aim of this study was to clarify the effect of aggregation behavior of casein micelles during *in vitro* digestion on the release of loaded ACNs, and to further utilize CCP and serum Ca²⁺ as the breakthrough to achieve precise release. In view of MC as a wall material, this study wishes to provide a facile and effective method to control the micelle structure and thus realize loaded ACNs in intestine with multiple release modes available.

2 Materials and methods

2.1 Materials

Anthocyanins (malvidin-3-O-glucoside 30.23% and delphinidin-3-O-glucoside 23.46% as two main anthocyanins) with a purity about 22% was obtained from Da Hinggan Mountains Lingebe Cold Zone Biotechnology Co., Ltd (Heilongjiang, China). Micellar casein powders (protein content 86.98%, fat content 1.41%, and lactose content 2.85%) were obtained from Ingredia Dairy Experts (Wapakoneta, OH, USA). Calcium chloride dihydrate (analytical reagent grade) was purchased from Macklin Biochemical Technology Co., Ltd. (Shanghai, China). Porcine pepsin (P7012, enzyme activity: 2500 U/mg) and pancreatin (P7545, enzyme activity: trypsin 200 U/mg, amylase 200 U/mg, and lipase 160 U/mg) were purchased from Sigma-Aldrich Chemical Company (St. Louis, MO, USA).

2.2 ACNs-MC encapsulation preparation

The MC dispersion (12% w/w) was stirred at 1000 rpm for 12 h at room temperature using a magnetic stirrer (RCT digital 2.07, IKA, Staufen, Germany) until fully hydrated. The MC dispersion was then atomized via a mini spray dryer (B-290, Büchi Labortechnik AG, Flawil, Switzerland) equipped with a two-fluid nozzle at a feed rate of 6 mL/min, and the diameters of the nozzle cap and the nozzle tip were 1.5 and 0.7 mm. To obtain droplets with large (SFD-L), medium (SFD-M), and small (SFD-S) particle sizes, the compressed air flow rate during atomization was set to 0, 138, and 831 L/h to achieve different freezing degrees. The droplet size measurement method was referred to in previous literature.²⁴ Specifically, the magenta solution (0.2%, w/v) was added after the MC dispersion was prepared. A petri dish (20 cm in diameter) containing dimethylsilicone oil was placed 10 cm below the nozzle as a container for the dyed droplets. Images were captured by a microscope (DM2500, Leica Microsystems GmbH, Wetzlar, Germany) and the particle

size of 100 droplets was sampled with ImageJ software (National Institutes of Health, Bethesda, MD, USA) and the mean values were calculated.

To obtain SFD samples, atomized droplets were sprayed into liquid nitrogen container set 10 cm below the nozzle tip. After that, the frozen droplets were immediately stored in an ultra-low temperature refrigerator until the liquid nitrogen was volatilized entirely. Finally, the collected ice crystals were freeze-dried for 24 h. Control samples prepared by spray drying (SD) and freeze drying (FD) were prepared using previous methods.^{25,26} Agglomerated particles were removed by a 180 µm stainless steel sieve. The obtained powders (SD, FD, SFD-L, SFD-M, SFD-S) were stored in a desiccator equipped with discolored silica gels for further utilization. The ratio of MC powders to blueberry ACNs extracts was set at 50:1²⁶ and dissolved in deionized water before being freeze-dried into powdery encapsulations.

2.3 Physicochemical properties of ACNs-MC powders

The encapsulation efficiency of powdered samples was measured as follows. Firstly, ACNs-MC powders (0.5 g) were dissolved into absolute methanol (15 mL). The mixtures were vortexed for 10 s and centrifuged at 12000 rpm for 10 min to obtain the supernatants, which were used to extract the ACNs on surface. The extraction solvent was replaced with mixtures (15 mL, anhydrous methanol:water = 2:1, v/v) to obtain the total ACNs. The ACNs-MC particles were destroyed with an ultrasonic cleaner before centrifuging at 12000 rpm for 10 min. This procedure was repeated three times to ensure that all ACNs were released. After that, the total ACNs in supernatants were detected by the pH differential method. Specifically, the supernatants were diluted to equal amounts of HAC-NaAc buffer solution (0.2 M, pH 4.5) and HCl-KCl buffer solution (0.2 M, pH 1.0), respectively. The absorbance values at 720 nm and 520 nm were detected by a microplate reader (Tecan Spark 10M, Tecan Trading AG, Switzerland). The encapsulation efficiency of ACNs-MC powders was calculated according to Eq. (1):

$$\text{Encapsulation efficiency (\%)} = \frac{(\text{total ACNs} - \text{surface ACNs}) / \text{total ACNs}}{\times 100} \quad (1)$$

The particle size of ACNs-MC powders was measured by a dynamic light scatterometer with the powder measurement module (FLOWSYNC, Microtrac MRB, PA, USA). A halogen moisture meter (HE83/02, Mettler Toledo Ltd., Greifensee, Switzerland) was used to measure the moisture content. The contents of serum Ca²⁺ and colloidal Ca²⁺ were analyzed using inductively coupled plasma optical emission spectrometry (ICP-OES) (Avio 200, PerkinElmer, Waltham, MA, USA). Powders (0.5 g) were dissolved in deionized water (50 mL) and centrifuged immediately after slight vortexing. The supernatants were then collected and centrifuged (4500 g, 30 min) in an ultrafiltration centrifuge tube (molecular retention: 3 kDa). The filtrate was used to measure the Ca²⁺ content as the serum Ca²⁺ level. Total Ca²⁺ level was measured as follows: Powders (0.5 g) were dissolved in deionized water (50 mL), and the concentration of Ca²⁺ in the solution was measured as the total Ca²⁺ level after

continuous stirring for 48 h. The relative content of the colloidal Ca^{2+} was calculated as Eq.(2):

$$\begin{aligned} \text{Relative colloidal } \text{Ca}^{2+} (\%) \\ = \frac{(\text{total } \text{Ca}^{2+} - \text{serum } \text{Ca}^{2+})}{\text{total } \text{Ca}^{2+}} \\ \times 100 \end{aligned} \quad (2)$$

2.4 *In vitro* static digestion of ACNs-MC

During *in vitro* digestion, a constant temperature water bath shaker (SHA-82A, Changzhou Guohua Electric Appliance Co., Ltd., Changzhou, China) was used to maintain a temperature of 37 °C and 120 rpm throughout the experiment. Conical flasks (100 mL) were used as containers to hold different digested samples. The digestion steps were based on the recommendations of INFOGEST 2.0 with some modifications²⁷. Electrolyte stock solutions of Simulated Gastric Fluid (SGF) and Simulated Intestinal Fluid (SIF) were prepared as described by Brodkorb et al.²⁷, and their composition is shown in Table S1†. During the digestion experiment, powder samples (2.5 g) were dispersed in SGF (50 mL) and stirred for 30 s to simulate the initial dissolution of powders before consumption. The pH of the mixture solution was then adjusted to 3.0, and pepsin and CaCl_2 solution were immediately added at final concentrations of 2000 U/mL and 0.15 mM, respectively. Gastric digestion was carried out for 2 h before adjusting the pH of simulated gastric chyme to 7.0. Simulated intestinal digestion started with the addition of an equal amount of SIF, and pancreatin, bile salt, and CaCl_2 solution were added to create another 2 h of intestinal digestion at final concentrations of 100 U/mL, 10 mM, and 0.6 mM in mixed SGF and SIF solution. Equal amounts of digesta were collected uniformly into transparent tubes at 5, 90, 125 and 210 min to observe dissolution and phase separation. Photographs were taken after 5 min of settling.

Particularly, to explore the effect of exogenous serum Ca^{2+} on the coagulation behavior of MC, SGF and SIF without CaCl_2 solution were used to treat those samples, which were compared as controls (N-SD, N-FD, N-SFD-L, N-SFD-M, N-SFD-S).

2.4.1 The release of ACNs during *in vitro* digestion.

The digesta collected at 5, 15, 30, 60, 90, 120, 125, 135, 150, 180, 210, and 240 min were placed on ice rapidly to inhibit enzyme activity. Then, anhydrous methanol was added to the digesta and centrifuged at 12000 rpm for 10 min to obtain the supernatants, which were further used to quantify the released ACNs according to the description in Section 2.3. The release rate was calculated following Eq.(3):

$$\begin{aligned} \text{Cumulative release } (\%) \\ = \frac{\text{released ACNs content in supernatants}}{\text{total ACNs content before digestion}} \\ \times 100 \end{aligned} \quad (3)$$

2.4.2 The dynamic dissolution of ACNs-MC during *in vitro* digestion

The digesta collected at 10, 30, 60, 90, 120, 130, 150, 180, 210, and 240 min were centrifuged at 3000 *g* for 10 min. Then the sediment was dried in an oven at 105 °C until reaching a constant weight. The weight of the dried solids was used to

calculate the concentration of undissolved solids in digestive fluid (*w/w*). Additionally, the digesta collected at 5, 90, 125 and 210 min were utilized to characterize the size distribution by a dynamic light scattering analyzer equipped with a wet module (FLOWSYNC, Microtrac MRB, Montgomeryville and York, PA, USA). During the test, the shading coefficient of each sample was stabilized at 0.3 ± 0.05 .

2.4.3 The serum Ca^{2+} level during gastric digestion

Digestion experiments with and without the addition of Ca^{2+} in the digestive electrolyte were carried out to monitor the serum Ca^{2+} level during gastric digestion. Firstly, digesta at 5 and 90 min were collected, and the same treatments as in Section 2.3 were performed. Then, serum Ca^{2+} level was determined using a Ca^{2+} selective electrode (perfectION™, Mettler Toledo Technology Co., Ltd., Zürich, Switzerland), which was calibrated in advance with Ca^{2+} standard solutions at concentrations of 10, 100, and 1000 mg/L. During the test, 50 mL of the solution to be tested was mixed with 1 mL of Ca^{2+} strength adjustment solution. The electrode was then immersed in the mixture, and serum Ca^{2+} level was read from the equipment screen.

2.4.4 SDS-PAGE patterns during *in vitro* digestion

To inactivate the enzymes, chyme was sampled at 5, 90, 125, and 210 min and placed in a boiling water bath for 5 min. Then they were vacuum freeze-dried and dissolved in a loading buffer to reach a concentration of 2.5 mg/mL. The PageRuler Prestained Protein Ladder (10–180 kDa, Thermo Fisher Scientific Inc., MA, USA) was used as a molecular weight marker. The loading amount for each lane of gel electrophoresis was fixed at 20 μL . Electrophoresis, staining, destaining, and imaging procedures were conducted using the method adopted in Yin et al.²⁸.

2.4.5 Degree of hydrolysis of ACNs-MC during *in vitro* digestion

The OPA (*o*-phthalaldehyde) method was used to quantify primary amino groups resulting from proteolysis during *in vitro* digestion. OPA reagents were prepared according to the method of Halabi et al.²⁹ Before testing, digesta collected at 5, 90, 125, and 210 min were centrifuged at 10,000 *g* for 15 min at 4 °C. The supernatant was diluted six times in PBS buffer with pH 7.0 and then 20 times in OPA reagent. Samples were then incubated for 5 min at 37 °C in a 96-well microtiter plate, and absorbance was measured at 340 nm with a microplate spectrophotometer (Multiskan™ GO, Thermo Fisher Scientific, Waltham, MA USA). Primary amino groups were quantified using a standard glycine curve over a concentration range of 0 to 16 mM. Degree of hydrolysis was calculated according to Eq.(4):

$$\begin{aligned} \text{Degree of hydrolysis } (\%) \\ = \frac{\text{NH}_2 \text{ digesta} - \text{NH}_2 \text{ secretions} - \text{NH}_2 \text{ undigested MC}}{\text{NH}_2 \text{ total} - \text{NH}_2 \text{ undigested MC}} \\ \times 100 \end{aligned} \quad (4)$$

where $\text{NH}_2 \text{ digesta}$ and $\text{NH}_2 \text{ undigested MC}$ are the primary amino groups in the samples after and before digestion. In gastric

digestion, NH_2 secretions are mainly considered as primary amino groups from pepsin. In intestinal digestion NH_2 secretions are mainly considered as primary amino groups from pepsin, pancreatin and bile salts. NH_2 total are the primary amino groups of the MC powders after hydrolysis with 6 M HCl at 110 °C for 24 h. The volume ratio of HCl to sample solution was 10:1. After acid hydrolysis, the acid was neutralized with 6 M NaOH in an equal volume with HCl.

2.4.6 The fluorescence spectrum of ACNs-MC during in vitro digestion

Digested samples at 5, 90, 125, and 210 min were centrifuged (10000 *g*, 10 min) to remove large curds. Then supernatants were collected for measurement of fluorescence intensity using a fluorescence spectrophotometer (F-280, Tianjin Gangdong Technology Co., Ltd., Tianjin, China). Before testing, all samples were diluted into the same concentration of 0.1 mg/mL by PBS buffer. The excitation wavelength was set to 280 nm, and the emission wavelength was set from 300 to 400 nm. The excitation and emission slit widths were both 5.0 nm. PBS background signals were subtracted from sample measurement results.

2.4.7 Structural changes of ACNs-MC characterized by WAXS/SAXS

Samples digested at 5, 90, 125, and 210 min were vacuum freeze-dried for measurement. Detailed structural changes of MC particles during digestion were monitored and characterized by WAXS/SAXS (Nano-inXider, Xenocs Scientific Instrument Technology Co., Ltd., Grenoble, France), which was equipped with a Cu K_α source and a two-detector setup for simultaneous WAXS/SAXS measurements with a 1.54 Å wavelength. The detector model of the instrument was PILATUS3 3×100K. Referring to Li et al.³⁰ and Yang et al.³¹, $q = 0.01 \text{ \AA}^{-1}$ (represents nanoclusters made of CCP cross-linked subunits, which have a particle size of about 20 nm) was taken as the dividing line. The scattering vector (q) was divided into low- q and high- q regions. The q - $I(q)$ curve was fitted in two segments by SasView software (version 5.0.3, <http://www.sasview.org/>) to obtain structure parameters. The model of Fractal-like Aggregates of Spheres was selected to fit the curve based on literature reported by Teixeira.³² Fractal is a geometric concept initially used to describe partitioning of oddly shaped objects and can be used to determine structure, composition, and formation process of gels. Specifically, the final scattering intensity $I(q)$ of spherical fractal aggregates was calculated according to Eq. (5).

$$I(q) = \phi V \rho^2 P(q) S(q) \quad (5)$$

where ϕ is the volume fraction of the spherical building block particles with radius R_0 , which reflects the strength of the interaction between the scattered particles (e.g., hydrophobic, electrostatic interactions and hydrogen bonds); ρ is the scattering length density, reflecting the amount of protein aggregations. V is the volume of a single building block, which was calculated as follow:

$$V = 4\pi R_0^3/3 \quad (6)$$

$P(q)$ is the scattering of randomly distributed spherical particles, of which the calculation formula was as follows:

$$P(q) = F(qR_0)^2 \quad (7)$$

$$F(q) = 3(\sin x - x \cos x)/x^3 \quad (8)$$

$S(q)$ is the interference caused by fractal clusters, and the calculation formula was as follows:

$$S(q) = 1 + \frac{D_f \Gamma(D_f - 1)}{[1 + 1/(q\xi)^2]^{(D_f - 1)/2}} \cdot \frac{\sin[(D_f - 1) \tan^{-1}(q\xi)]}{(qR_0)^{D_f}} \quad (9)$$

where ξ represents the length of the cluster, which reflects the size of the scattered particles; D_f is the fractal dimension, which reflects the roughness and compactness of the structure. The surface fractal ($3 \leq D_f \leq 4$) represents particles with rough or smooth surface, where D_f is positively correlated with surface roughness. The mass fractal ($1 \leq D_f \leq 3$) represents the particles with branching and cross-linking network structure, in which D_f is positively correlated with the compactness of the structure.

3 Results and discussion

3.1 Physicochemical properties of ACNs-MC encapsulation

As shown in Table S2[†] and Table 1, the droplet size of SFD samples (2910.3, 138.0, 3.5 μm) was positively correlated with colloidal Ca^{2+} levels in their powders (79.4%, 47.8%, 40.2%). Small droplets imply a higher freezing degree compared to larger droplets. Therefore, more Ca^{2+} from the colloidal phase in SFD-S was transferred to serum phase comparing to SFD-L and SFD-M. The colloidal Ca^{2+} level of SFD-L (79.4%) was close to the controlled SD (80.4%) and FD (77.8%) samples. In addition, the encapsulation efficiency of ACNs increased from 49.1% to 60.8% with the decrease of colloidal Ca^{2+} level. CCP dissociation induced by the Ca^{2+} interphase transition led to more nanoclusters in solution. These clusters possessed a high specific surface area and hence an increasing binding opportunity with ACNs.³³ After lyophilization into powdery form, all samples showed a similar particle size (135.1–142.0 μm). The moisture content of all powders was less than 3.7%, which suggests that they showed a favorable storage stability.

Table 1 Physicochemical properties of ACNs-MC encapsulation.

Sample	SD	FD	SFD-L	SFD-M	SFD-S
Relative percentage of colloidal Ca ²⁺ (%)	80.4 ± 0.5 ^a	77.8 ± 0.8 ^a	79.4 ± 1.1 ^a	47.8 ± 1.1 ^b	40.2 ± 0.1 ^c
Encapsulation efficiency (%)	41.1 ± 1.0 ^e	47.1 ± 0.4 ^d	49.1 ± 1.1 ^c	53.7 ± 0.9 ^b	60.8 ± 0.2 ^a
Particle size D(50) (µm)	137.2 ± 1.2 ^{ab}	138.2 ± 1.3 ^{ab}	142.0 ± 3.5 ^a	135.1 ± 1.5 ^b	138.6 ± 2.3 ^{ab}
Moisture content (%)	3.2 ± 0.0 ^d	3.7 ± 0.0 ^a	3.6 ± 0.0 ^b	3.5 ± 0.1 ^c	3.2 ± 0.0 ^d

Values with different superscript letters in each column are significantly different ($p < 0.05$).

3.2 The dynamic release of ACNs during *in vitro* digestion

The release of ACNs in gastrointestinal digestion is shown in Fig. 1A and Fig. 1B. When Ca²⁺ was added, the release of ACNs was inhibited due to the intensified CCP dissociation. Especially for the SFD-S sample, just about 15% of ACNs was released at 120 min. After entering the intestine, the release of ACNs remained slow and consistent, which increased from 15% to 65% within 2 h. In contrast, SD and FD samples showed about 35% release into supernatant in stomach. Once entering intestine, the ACNs released explosively from 35% to 90% within 5 min. SFD-L showed similar release behavior in intestinal tract, but it protected ACNs in stomach. When serum Ca²⁺ was absent, ACNs exhibited a relatively high release throughout the digestion process.

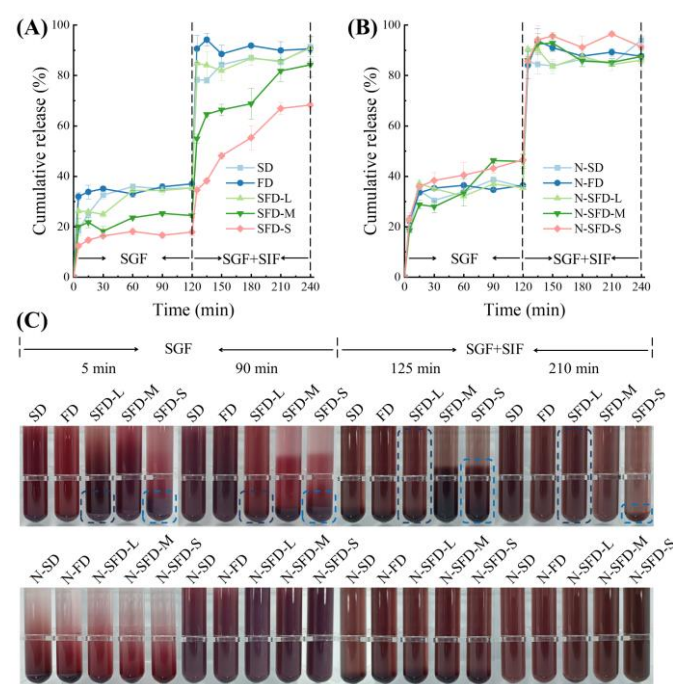


Fig. 1 Release of anthocyanins during *in vitro* digestion with (A) and without (B) addition of exogenous serum Ca²⁺ to simulated gastric fluid and the appearance of the digesta (C).

Fig. 1C illustrates the dissolution and phase separation of ACNs-MC during *in vitro* digestion. In gastric digestion, phase separation could be clearly observed in SFD-S sample. It was

particularly noted that large amounts of purple curd appeared at the bottom of the tube, which was distinctly separated from the pink supernatant. At 125 min, the curds in bottom disappeared and turned into dark purple precipitates, which significantly more than others, while the supernatant appeared lavender. At the end of intestinal digestion (210 min), only SFD-S remained slightly precipitated, and its supernatant color was obviously lighter than others. Additionally, SFD-L also generated some small amounts of curd in gastric tract, and its supernatant color presented between FD and SFD-M. However, SFD-L exhibited a closer color in intestine to SD and FD samples, which agrees with the results in Fig. 1A. N-SFD samples showed tremendous color variation from 5 min to 90 min. At 5 min, the phase separation of the digesta was obvious. The supernatant was almost clear and contained few curds at the bottom of the tube. However, the digesta of 90 min turned into a homogeneous dark red liquid. In intestine, N-SFD was observed as a small amount of precipitate merely at the beginning (125 min), and it showed a homogeneous purple liquid later.

It should be noted that Fig. 1C was taken after 5 min of settling, so layering occurred in tubes according to the size of aggregates, which means that the release of ACNs could be evaluated by the supernatant color. ACNs served as the model core material in this study, and its release behavior was closely related to the digestion behavior of the wall material. ACNs were effectively loaded as water-soluble pigments inside the micelle structure, whose release was hindered by the barrier provided by the wall material. In acidic environment of the stomach, the cationic form of ACNs in 2-phenylchromen contributed to the red color of the digesta.³⁴ Due to high levels of serum Ca²⁺ in SGF, internal ACNs could be abundantly retained in undissolved dark red curds to avoid release, thus leading to slow release in small intestine. At intestinal phase, the curds at the bottom of the tube almost disappeared. Aggregates were rapidly hydrolyzed or dissolved into massive dark purple (methanolic pseudobase or chalcone forms of ACNs) precipitates.³⁵ Because of the abundant precipitation, it could be retained until the end of digestion to provide sustained release of ACNs in intestinal tract. In contrast, for those samples with less curd formation in stomach, it tended to release significant amounts of ACNs at the early stages of intestinal digestion.

3.3 The dynamic dissolution of ACNs-MC during *in vitro* digestion

As shown in Fig. 2A, the dissolution of SFD-S sample remained stable at about 40% during the gastric phase, while other samples decreased continuously from 55–60% to about 40–50%. It indicates that the aggregates of SFD-S sample were formed faster than others, but the content was almost the same. Yet at the intestinal phase, the solubility of each sample showed remarkable differences. SFD-S sample exhibited a strong resistance to dissolution, as just 40% of the aggregates were dissolved within 120 min, while SD, FD and SFD-L showed approximately 60%. When excluding adding exogenous serum Ca²⁺, all samples reached more than 90% solubility at the end of gastric digestion and were almost completely dissolved at just

10 min into intestinal tract (Fig. 2B), which corroborates the phenomenon observed in Fig. 1C. As can be seen in Fig. 2C, the size distribution of SFD-S sample tended to concentrate more in large-sized regions. Even at the late stage of intestinal digestion, the size remained centered at about 70 μm , while SD, FD, and SFD-L samples showed all just around 0.1 μm . Moreover, SFD-M showed similar distribution as SFD-S sample, while SFD-L resembled FD and SD samples more. It was similar to the release pattern of ACNs presented in Fig. 1A and Fig. 1C, which verified the potential correlation between the release pattern of core ACNs and the solubility profile of wall MC in intestine. The size distribution of ACNs-MC in stomach without the addition of exogenous serum Ca^{2+} was significantly reduced to about 20–30 μm , which was over 10 times smaller than SFD-S sample. After that, it decreased to about 1 μm just as it entered the intestinal phase. It strongly demonstrates that serum Ca^{2+} level had a considerable impact on the amount of gastric coagulum generation and the capacity to resist intestinal hydrolysis.

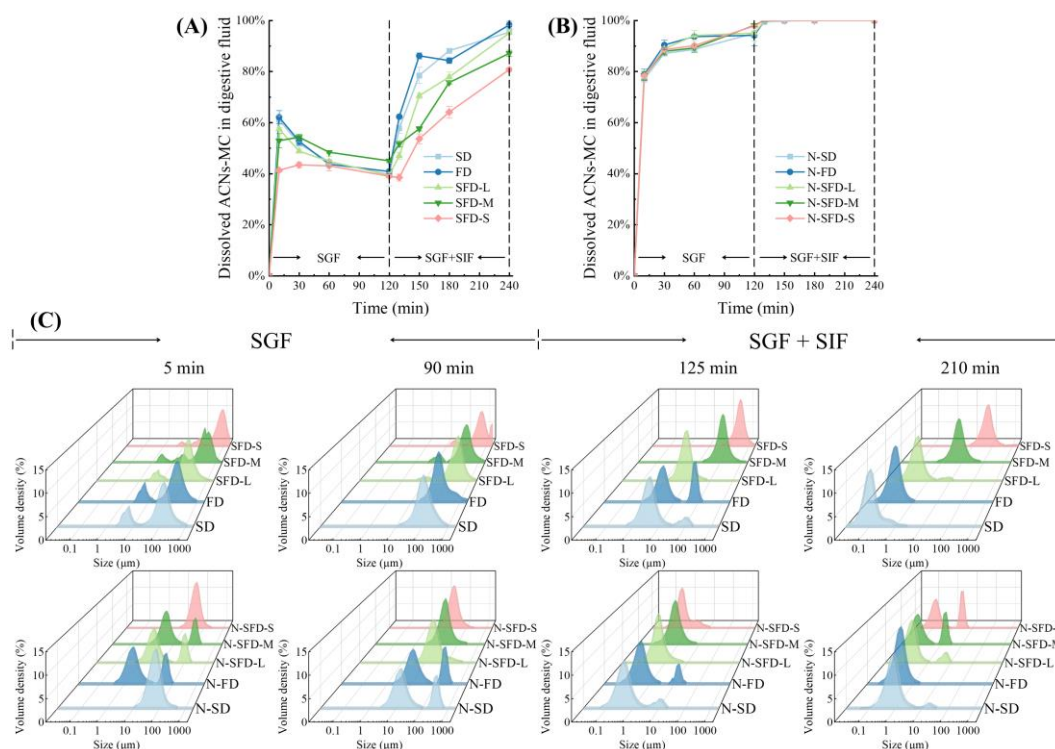


Fig. 2 Dynamic dissolution of ACNs-MC during *in vitro* digestion with (A) and without (B) addition of exogenous serum Ca^{2+} in simulated gastric fluid; The size distribution (C) of ACNs-MC during *in vitro* digestion. The prefix 'N-' represents the absence of exogenous serum Ca^{2+} in gastric fluid of the corresponding sample.

3.4 The serum Ca^{2+} level during gastric digestion

Due to the sensitivity of wall MC to serum Ca^{2+} and the possibility that serum Ca^{2+} inherent in SGF may disrupt the equilibrium between the colloidal and serum phases, the utilization of serum Ca^{2+} during the early and late gastric digestion was evaluated. In order to compare serum Ca^{2+} consumption in stomach of each sample, serum Ca^{2+} levels in SGF with and without exogenous Ca^{2+} addition were measured during gastric digestion and their difference (Δ) was calculated (Fig. 3). Lower Δ values indicated that more serum Ca^{2+} was involved in the formation of aggregates. The highest Ca^{2+} consumption was observed in SFD-S at 5 min, with a Δ value of just 55 mg/L. The other samples ranged from 1.5–2.5 times higher than this value. As digestion proceeded to 90 min, Ca^{2+} was significantly reduced in all samples. In particular, SFD-S remained the highest Ca^{2+} consumption among all samples. The other samples ranged from 2–4.8 times higher than SFD-S. Significant differences ($p < 0.05$) were also observed among SFD-L, SFD-M and SFD-S. It suggests that CCP level of these samples had a significant effect on the consumption of serum Ca^{2+} during gastric tract. With the addition of exogenous serum Ca^{2+} in SGF, the phase equilibrium $\text{Ca}_3(\text{PO}_4)_2 \downarrow + 2\text{H}^+ \rightleftharpoons 2\text{HPO}_4^{2-} + 3\text{Ca}^{2+}$ within micelle structure spontaneously shifted to the colloidal phase (left), which led to more CCP reassembled.¹⁴ Meanwhile, Ca^{2+} reduction might be related to the exposure of phosphorylated serine residues. Since CCP dissociation was accompanied by the release of MC subunits and an increase in specific surface area, the Ca^{2+} -binding sites on subunits were exposed more and facilitated binding opportunities improved.

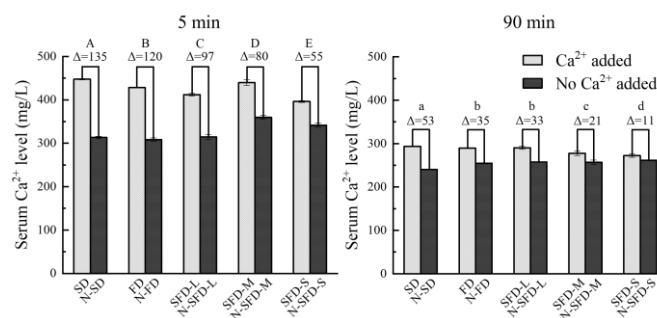


Fig. 3 The serum Ca^{2+} level during gastric digestion with and without adding Ca^{2+} in the digestive electrolyte. The prefix 'N-' represents the absence of exogenous serum Ca^{2+} in gastric fluid of the corresponding sample. The different letters on the bars indicate the significant difference ($p < 0.05$) of the results in same group.

3.5 SDS-PAGE patterns during *in vitro* digestion

For characterizing the proteolysis of MC as wall material during digestion and the possible subunit cross-linking mediated by serum Ca^{2+} in stomach, SDS-PAGE experiments under reducing conditions were performed. With the presence of exogenous Ca^{2+} in stomach, SDS-PAGE patterns were mainly at 50 kDa and above, including the stacked bands over 180 kDa and the band around 50–60 kDa (Fig. 4). These bands were the deepest in SFD-S lane during the whole gastric process, followed by SFD-M sample. However, only two bands at around 20 kDa could be observed clearly in N-SFD samples, and the bands at 50 kDa (and above) were not obvious and even tended to disappear in late gastric digestion. It strongly illustrates that serum Ca^{2+} addition greatly influenced the gastric aggregation behavior of wall MC, which

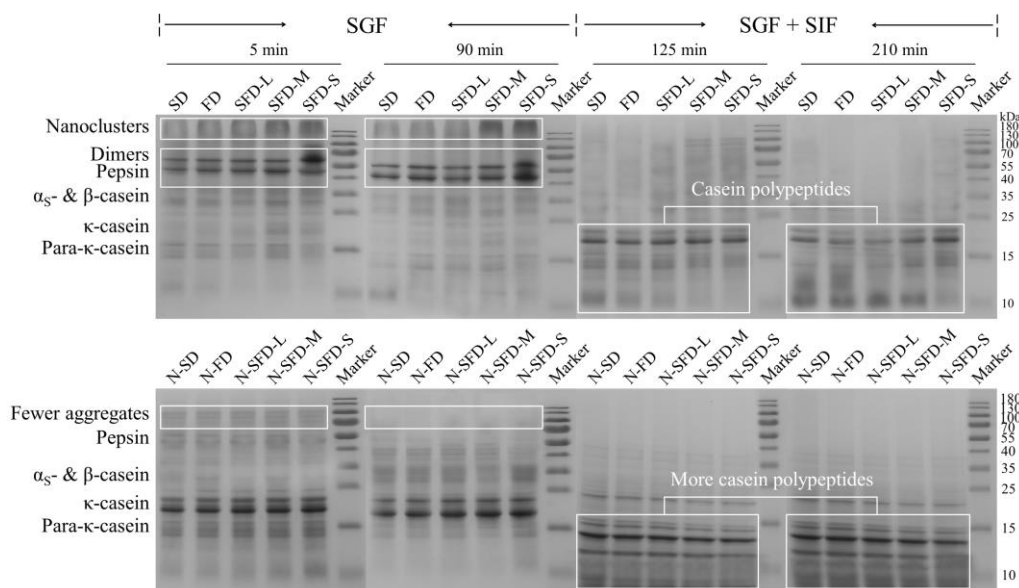


Fig. 4 SDS-PAGE patterns under reducing conditions during *in vitro* digestion. The prefix 'N-' represents the absence of exogenous serum Ca^{2+} in gastric fluid of the corresponding sample.

also showed a potential correlation with CCP level. In intestine phase, SFD-S and SFD-M samples showed a series of retention bands at 30–100 kDa, while at 10–15 kDa were shallower than others. However, protein bands at 15 kDa (and below) were significantly deepened without adding serum Ca^{2+} , and the extent of proteolysis was roughly similar among samples. As discussed in Section 3.4, the bands above 180 kDa were probably nanoclusters formed by serum Ca^{2+} involved in reconstituting CCP and then re-crosslinking MC subunits.³⁶ According to previous studies, the bands around 50–60 kDa could be crosslinkers between the homologous MC subunits, that was α_s -casein dimer and β -casein dimer.^{37–40} Due to the higher involvement of Ca^{2+} for cross-linking reactions within SFD-S sample, its clusters showed stronger resistance to hydrolysis. Nevertheless, electrophoresis tests could not accurately reflect the degree of hydrolysis. Consequently, tests that can accurately quantify the degree of hydrolysis are performed in the following to verify the observations in this section.

3.6 Proteolysis during *in vitro* digestion

The degree of hydrolysis of MC was quantified by determining its free amino acid level. In Fig. 5A and Fig. 5B, all samples exhibited a low degree of hydrolysis (3%–15%) in gastric phase, especially the SFD samples (9%, 7% and 3%), which presented the same result as the CCP levels. At just 5 min into intestinal phase, they already showed very different degrees of hydrolysis. SFD-S and SFD-M were at about 18%, while SFD-L was close to SD and FD at about 70%. Later at 210 min in intestine, SFD-L showed little change, while SFD-S increased slightly to about 23% and SFD-M elevated to about 35%. The samples without serum Ca^{2+} addition all exhibited rapid intestinal hydrolysis characteristics, and their degree of hydrolysis was similar to the SFD-L. Fluorescence test of digesta was also applied to characterize the hydrolysis degree. Fluorescence intensity of

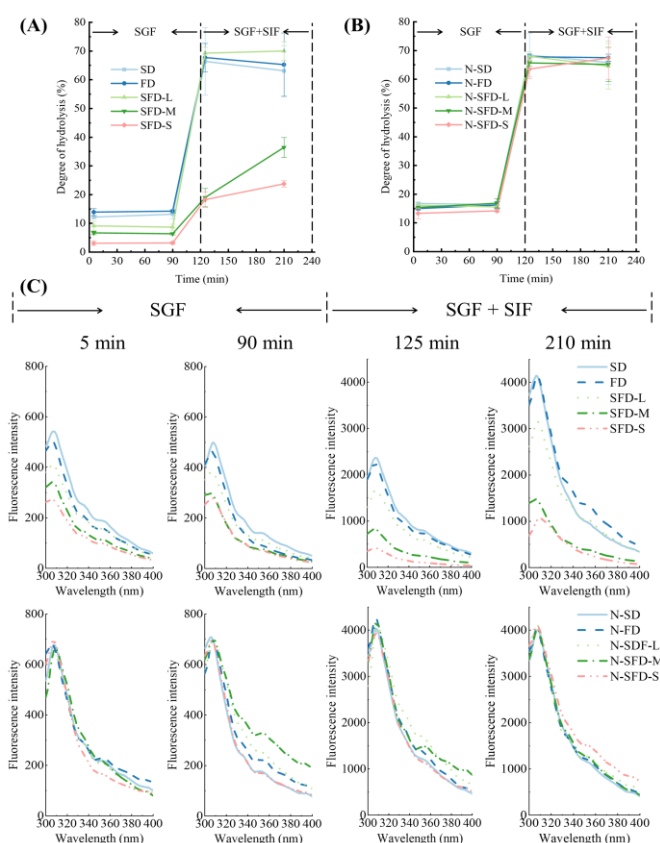


Fig. 5 Degree of hydrolysis of ACNs-MC during *in vitro* digestion in gastric fluid with (A) and without (B) exogenous serum Ca^{2+} ; (C) The fluorescence spectrum of ACNs-MC during *in vitro* digestion. The prefix 'N-' represents the absence of exogenous serum Ca^{2+} in gastric fluid of the corresponding sample.

ACNs-MC reflected the exposure of endogenous hydrophobic amino acids (tryptophan, leucine, phenylalanine, etc.).⁴¹ Samples were highly affected by pyrolysis showed a significant

increase in fluorescence intensity, which reflected the reduced structural integrity of their wall materials.⁴² In Fig. 5C, SFD-S with the highest degree of CCP dissociation exhibited the lowest fluorescence intensity in stomach, which revealed the relatively intact structure of gastric aggregates it formed. After entering intestine, the fluorescence intensity of all samples increased significantly. Among them, the intensity value of SFD-S remained the lowest, which was about one-third of SFD-L. While the fluorescence intensities of N-SFD samples were relatively comparable and high.

Changes in hydrolysis of ACNs-MC during *in vitro* digestion showed substantial consistency with the observations in Section 3.5. It indicates that enhanced reconstruction from low CCP level tended to exhibit stronger resistance to hydrolysis and maintain a complete gastric aggregation structure. Combined with the *in vitro* release measurements in Section 3.2, it was noted that intestinal hydrolysis behavior of aggregates correlated with the release pattern of ACNs, of which SFD-M and SFD-S exhibited slow release. Surprisingly, the gastric aggregates of SFD-L sample showed resistance to hydrolysis and exhibited some protection to ACNs in Fig. 1. However, it showed great burst release performance in following intestinal phase and differed from SFD-S and SFD-M samples. High levels of release (from 32% to 83%) were reached at 5 min after entering intestine. Therefore, casein micelles with low CCP dissociation have potential as delivery carriers for intestinal burst cores.

3.7 Structural changes of ACNs-MC during *in vitro* digestion

It has been demonstrated above that MC as wall material bound to other particles in stomach via serum Ca^{2+} and subsequently aggregates, and its binding amount was related to the CCP level. Meanwhile, the dissolution and hydrolysis of the generated aggregates in intestine influenced the release pattern of core ACNs. In this section, WAXS/SAXS was used to characterize the structure of wall MC in delivery system during digestion. It aims to fully investigate structural changes of the aggregates and structural differences of MC with different CCP level during *in vitro* digestion. The analysis will be focused on structural changes after cross-linking Ca^{2+} .

Fig. 6 shows the q - $I(q)$ profiles of the aggregates in full scale range. At the same gastric digestion time, it was noted that the q - $I(q)$ profiles of SFD-S and N-SFD-S samples were significantly decreased with adding exogenous serum Ca^{2+} . It indicates that micelle structure of SFD-S was most markedly influenced by the level of serum Ca^{2+} . In conjunction with the results in Fig. 3, it could be due to the full unfolding of SFD-S micelle structure and thus more Ca^{2+} -binding sites exposure. As described in Section 3.4, high serum Ca^{2+} levels shifted the phase equilibrium $\text{Ca}_3(\text{PO}_4)_2 \downarrow + 2\text{H}^+ \rightleftharpoons 2\text{HPO}_4^{2-} + 3\text{Ca}^{2+}$ towards the colloidal phase (left). Then, the repaired CCP acted as a bridge to crosslink the surrounding MC subunits to form aggregates. However, the q - $I(q)$ profile did not show the characteristic peak of CCP at $q = 0.08 \text{ \AA}^{-1}$.^{43–45} It might be related to the remodeling of micelle structure by gastric acid and pepsin, which together led to the co-existence of multiple types and multiple sizes of aggregates in digesta. As a result, multiple local fluctuations in density were generated during the experiment.^{46,47} Accordingly,

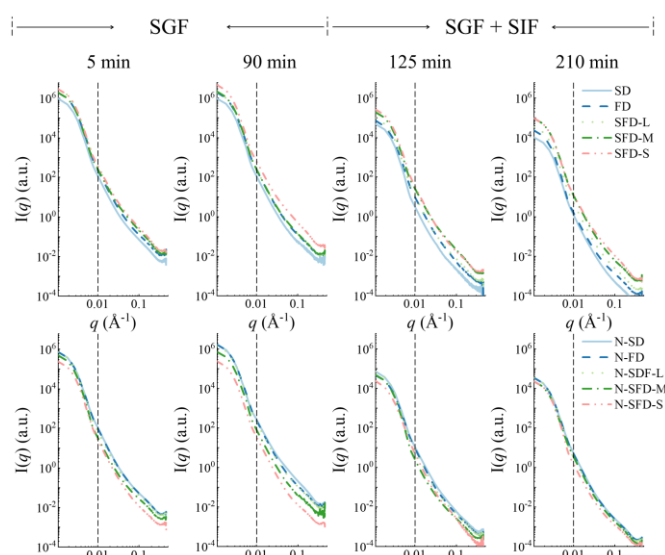


Fig. 6 WAXS/SAXS scattering profiles of ACNs-MC during *in vitro* digestion. The prefix 'N-' represents the absence of exogenous serum Ca^{2+} in gastric fluid of the corresponding sample.

the $I(q)$ value changed over the full range of q -scale, rather than merely relating to the region corresponding to CCP.

The scattering vector (q) was divided into low q and high q regions based on $q = 0.01 \text{ \AA}^{-1}$ as the dividing line. It corresponds to nanoclusters composed by CCP cross-linked subunits with particle size of about 20 nm.⁴⁸ In Table 2 and Table 3, the precise structure of the aggregates is elucidated by the parameters obtained from fitting the q - $I(q)$ profiles in two regions. The low- q region ($q < 0.01$) was taken as the structural analysis of aggregates in stomach (5 min, 90 min) and early intestinal digestion (125 min). Meanwhile, the high- q region ($q > 0.01$) was resolved as the structure of aggregates in intestine (210 min). ξ and R_0 are both parameters that describe the size of individual particles. They reflected the formation of aggregates in stomach and their dissolution or hydrolysis in intestine. The results in Table 2 and Table 3 generally agree with Fig. 2C that the particle size was negatively correlated with the CCP dissociation degree. ρ indicates the density of particles forming aggregates, which reflects the formation process. SFD-L, SFD-M and SFD-S samples showed an opposite trend of parameter ρ in low- q and high- q regions with the extension of gastric digestion. It reflects the fact that aggregates were formed by progressive cross-linking of casein subunits. Since the micelle surface was no longer restricted by κ -casein⁴⁹, the nanoclusters in high- q region could gradually enter to low- q region accompanied by the cross-linking of serum Ca^{2+} . D_f indicates the particle morphology, which reflects the surface roughness of gastric aggregates and structural tightness of remained particles in intestine. D_f in intestine could also be attributed to the severity of particle erosion due to dissolution or hydrolysis. As shown in Table 2, SFD-S exhibits the largest D_f value (3.6), which might be due to its extensive cross-linking of other particles in SGF. In intestinal digestion, the compactness of its structure (3.5) was greater than SFD-L (3.0). ϕ characterizes the strength of interparticle interactions, which evaluated the strength of electrostatic

Table 2 Structural parameters obtained from fitting the low- q region ($q < 0.01$) of WAXS/SAXS scattering profiles of ACNs-MC during *in vitro* digestion.

5 min - SGF - $q < 0.01$	SD	FD	SFD-L	SFD-M	SFD-S	N-SD	N-FD	N-SFD-L	N-SFD-M	N-SFD-S
Cluster correlation length (ξ) [Å]	211	218	249	402	443	264	232	233	230	218
Radius of particles (R_0) [Å]	320	331	304	316	355	311	300	303	300	306
Scattering length density (ρ) [$\times 10^{-6}$ Å $^{-2}$]	2.8	1.6	3.9	6.0	6.2	2.1	2.0	2.0	1.8	1.9
Fractal dimension (D_f)	3.1	3.3	3.2	3.4	3.6	3.0	3.0	3.1	3.1	3.0
Volume fraction of blocks (ϕ)	0.072	0.078	0.080	0.148	0.153	0.064	0.070	0.059	0.026	0.037
90 min - SGF - $q < 0.01$	SD	FD	SFD-L	SFD-M	SFD-S	N-SD	N-FD	N-SFD-L	N-SFD-M	N-SFD-S
Cluster correlation length (ξ) [Å]	215	218	328	434	441	230	231	225	228	218
Radius of particles (R_0) [Å]	303	301	294	356	363	312	290	301	300	306
Scattering length density (ρ) [$\times 10^{-6}$ Å $^{-2}$]	2.8	1.5	3.6	6.2	7.6	1.7	2.2	2.1	1.7	1.9
Fractal dimension (D_f)	3.1	3.2	3.2	3.5	3.6	3.2	3.1	3.2	3.1	3.0
Volume fraction of blocks (ϕ)	0.049	0.048	0.160	0.174	0.192	0.044	0.043	0.056	0.037	0.029
125 min - SGF+SIF - $q < 0.01$	SD	FD	SFD-L	SFD-M	SFD-S	N-SD	N-FD	N-SFD-L	N-SFD-M	N-SFD-S
Cluster correlation length (ξ) [Å]	207	218	240	432	431	218	200	187	186	178
Radius of particles (R_0) [Å]	306	300	295	354	362	302	299	300	303	301
Scattering length density (ρ) [$\times 10^{-6}$ Å $^{-2}$]	1.4	1.3	2.6	3.1	4.2	1.4	1.3	1.0	1.5	0.9
Fractal dimension (D_f)	3.0	3.1	3.0	3.4	3.5	2.9	2.7	2.8	2.7	2.8
Volume fraction of blocks (ϕ)	0.043	0.045	0.055	0.098	0.114	0.008	0.007	0.013	0.021	0.025
210 min - SGF+SIF - $q < 0.01$	SD	FD	SFD-L	SFD-M	SFD-S	N-SD	N-FD	N-SFD-L	N-SFD-M	N-SFD-S
Cluster correlation length (ξ) [Å]	117	135	156	240	383	94	94	93	97	93
Radius of particles (R_0) [Å]	306	298	295	354	361	302	295	307	298	298
Scattering length density (ρ) [$\times 10^{-6}$ Å $^{-2}$]	1.1	1.1	1.5	2.6	3.2	1.0	1.1	0.9	0.8	0.8
Fractal dimension (D_f)	2.9	3.0	3.0	3.3	3.4	2.4	2.4	2.2	2.3	2.2
Volume fraction of blocks (ϕ)	0.008	0.006	0.006	0.054	0.056	0.004	0.005	0.006	0.004	0.007

Fitting quality was evaluated using χ^2 . In this table, $1 < \chi^2 < 5$.

Table 3 Structural parameters obtained from fitting the high- q region ($q > 0.01$) of WAXS/SAXS scattering profiles of ACNs-MC during *in vitro* digestion.

5 min - SGF - $q > 0.01$	SD	FD	SFD-L	SFD-M	SFD-S	N-SD	N-FD	N-SFD-L	N-SFD-M	N-SFD-S
Cluster correlation length (ξ) [Å]	1.4	1.5	1.5	1.8	2.6	1.5	1.4	1.3	1.3	1.3
Radius of particles (R_0) [Å]	4.7	5.3	5.2	6.8	7.0	2.7	1.1	1.1	1.9	2.2
Scattering length density (ρ) [$\times 10^{-6} \text{Å}^{-2}$]	2.0	1.5	3.8	6.5	7.1	2.2	2.1	2.0	2.1	1.9
Fractal dimension (D_f)	2.9	2.9	2.9	3.0	3.0	3.0	2.9	3.0	2.9	2.7
Volume fraction of blocks (ϕ)	0.065	0.067	0.079	0.148	0.162	0.085	0.058	0.062	0.044	0.038
90 min - SGF - $q > 0.01$	SD	FD	SFD-L	SFD-M	SFD-S	N-SD	N-FD	N-SFD-L	N-SFD-M	N-SFD-S
Cluster correlation length (ξ) [Å]	1.4	1.6	1.9	1.8	2.5	1.5	1.2	1.5	1.3	1.3
Radius of particles (R_0) [Å]	4.7	5.4	5.0	6.1	7.2	2.5	1.0	1.3	1.9	2.2
Scattering length density (ρ) [$\times 10^{-6} \text{Å}^{-2}$]	3.0	2.7	1.9	1.5	1.3	2.2	2.1	2.3	2.5	2.0
Fractal dimension (D_f)	2.9	2.9	2.9	3.0	3.0	3.0	2.9	3.0	2.9	2.9
Volume fraction of blocks (ϕ)	0.059	0.063	0.065	0.169	0.184	0.069	0.052	0.057	0.050	0.049
125 min - SGF+SIF - $q > 0.01$	SD	FD	SFD-L	SFD-M	SFD-S	N-SD	N-FD	N-SFD-L	N-SFD-M	N-SFD-S
Cluster correlation length (ξ) [Å]	1.5	1.5	1.5	1.8	2.4	1.5	1.4	1.5	1.4	1.3
Radius of particles (R_0) [Å]	4.7	5.4	5.7	6.1	7.2	2.6	1.0	1.4	1.9	2.2
Scattering length density (ρ) [$\times 10^{-6} \text{Å}^{-2}$]	4.0	3.6	3.1	1.9	1.8	4.6	4.8	4.2	5.2	5.8
Fractal dimension (D_f)	2.5	2.4	2.5	3.0	3.0	3.0	2.9	3.0	2.9	3.0
Volume fraction of blocks (ϕ)	0.034	0.034	0.033	0.074	0.105	0.004	0.000	0.002	0.003	0.004
210 min - SGF+SIF - $q > 0.01$	SD	FD	SFD-L	SFD-M	SFD-S	N-SD	N-FD	N-SFD-L	N-SFD-M	N-SFD-S
Cluster correlation length (ξ) [Å]	1.5	1.5	1.6	2.1	2.3	1.4	1.4	1.5	1.4	1.4
Radius of particles (R_0) [Å]	4.4	5.2	5.6	6.2	7.6	2.1	1.3	1.8	1.9	2.2
Scattering length density (ρ) [$\times 10^{-6} \text{Å}^{-2}$]	6.3	6.5	6.3	6.0	4.8	5.7	5.9	5.6	5.6	5.7
Fractal dimension (D_f)	2.5	2.4	2.5	2.8	3.0	3.0	2.9	3.0	2.9	3.0
Volume fraction of blocks (ϕ)	0.011	0.012	0.013	0.061	0.077	0.001	0.001	0.000	0.001	0.005

Fitting quality was evaluated using χ^2 . In this table, $1 < \chi^2 < 5$.

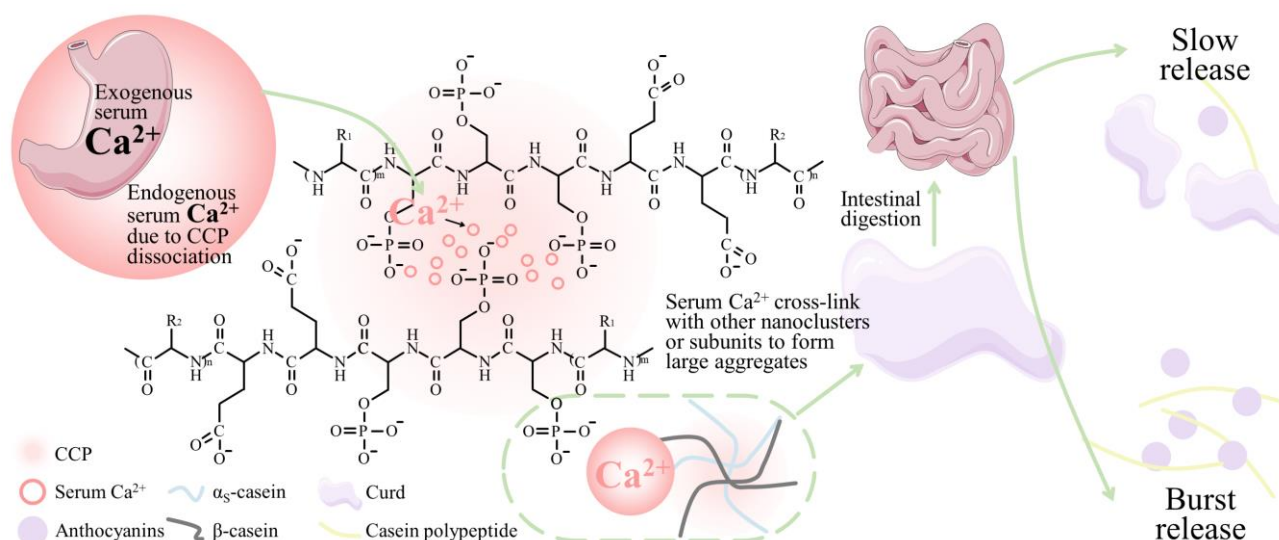


Fig. 7 Mechanism of gastric aggregation triggered by serum Ca^{2+} regulating the release pattern of anthocyanins.

interactions mediated by serum Ca^{2+} within the aggregates. ϕ values of SFD samples (0.160, 0.174, 0.192) were significantly higher than SD and FD samples (0.049, 0.048) at 90 min. However, ϕ value of SFD-L decreased to 0.033 at the beginning of intestinal phase, which is one-third of SFD-S sample. At 210 min, its ϕ value dropped further to 0.013, which is just one-sixth of SFD-S sample. The results about ϕ suggest that SFD-L sample severely hydrolyzed and solubilized in intestine, and its resistance was significantly weaker than SFD-S.

3.8 Mechanism of gastric aggregation regulating the release pattern of anthocyanins

In Fig. 7, the delivery system in this study was constructed as follows: Initially, casein micelles were subjected to different freezing degrees in SFD and MC with different CCP levels were obtained as wall materials. ACNs were then loaded and lyophilized to fix the partially dissociated micelle structure. In stomach, exogenous serum Ca^{2+} in SGF together with endogenous serum Ca^{2+} due to CCP dissociation recombined with phosphorylated serine residues, which aimed to reconstituted CCP-mediated nanoclusters. After that, these nanoclusters crosslinked with other nanoclusters or subunits via serum Ca^{2+} to form large aggregates. The anti-hydrolysis degree of the aggregates was controlled by serum Ca^{2+} level in ACNs-MC. During intestinal digestion phase, the release pattern of ACNs was obviously regulated by the anti-hydrolytic capacity of gastric aggregates. The sample with the highest serum Ca^{2+} level (SFD-S) exhibited as slow release, while the sample with a lower serum Ca^{2+} level (SFD-L) released ACNs explosively in small intestine.

4 Conclusion

In vitro, ACNs-MC delivery system designed in this study was well able to overcome the harsh acidic environment in stomach and the hydrolysis by pepsin. Based on this, the release pattern could be regulated by simply adjusting the droplet size of SFD.

The study was conducted using the static *in vitro* digestion method (INFOGEST 2.0)²⁷ for experimental manipulation. Although this method is widely used by researchers, it has some shortcomings compared to *in vivo*/dynamic/semi-dynamic methods such as shear force, enzyme and pH control, food flow and other factors that can affect experimental results.⁵⁰ These factors should be fully considered.

In this study, the design of the delivery system is based on the MC as the wall material. In the future, the SFD parameters as the 'down' can be adjusted according to the demand of the disease as the 'top', thus regulating the release pattern of the core material on demand. Moreover, SFD as a means of regulating wall MC avoids the introduction of chemical components with health risks in intermediate steps of sample preparation. As a pharmaceutical manufacturing process, which creates favorable conditions for long-term oral intake by patients; While as a health food manufacturing process, such clean-label compliant products are more beneficial to be embraced by consumers. The SFD technology applied in this study has been implemented in pharmaceutical field for high throughput production, however, its high-cost problem needs to be urgently overcome.

Author Contributions

Jinbo Ren: Formal analysis, Investigation, Visualization, Writing - original draft. **Minjie Liao:** Writing - review & editing, Investigation. **Kaixin Li:** Writing - review & editing, Investigation. **Fang Chen:** Supervision, Funding acquisition. **Xiaosong Hu:** Supervision, Funding acquisition. **Lingjun Ma:** Formal analysis, Resources, Supervision. **Junfu Ji:** Supervision, Conceptualization, Writing - review & editing.

Conflicts of interest

The authors declared no conflicts of interest.

Acknowledgements

The study was supported financially by National Key Research and Development Program of China (grant no. 2023YFF1104003) and National Natural Science Foundation of China (32372360, 32101983). Moreover, this work benefited from using the SasView application, originally developed under NSF Award DMR - 0520547. SasView also contains code developed with funding from the EU Horizon 2020 programme under the SINE2020 project Grant No 654000.

References

- 1 A. Abramson, S. Caffarel, M. Khang, D. Dellal, D. Silverstein, Y. Gao, M. Frederiksen, A. Vegge, F. Hubálek, J. Water, A. Friderichsen, J. Fels, R. Kirk, C. Cleveland, J. Collins, S. Tamang, A. Hayward, T. Landh, S. Buckley, N. Roxhed, U. Rahbek, R. Langer and G. Traverso, An ingestible self-orienting system for oral delivery of macromolecules, *Science*, 2019, **363**, 611–615.
- 2 X. Li, S. Jafari, F. Zhou, H. Hong, X. Jia, X. Mei, G. Hou, Y. Yuan, B. Liu, S. Chen, Y. Gong, H. Yan, R. Chang, J. Zhang, F. Ren and Y. Li, The intracellular fate and transport mechanism of shape, size and rigidity varied nanocarriers for understanding their oral delivery efficiency, *Biomaterials*, 2023, **294**, 121995.
- 3 U. Agrawal, R. Sharma, M. Gupta and S. Vyas, Is nanotechnology a boon for oral drug delivery?, *Drug Discovery Today*, 2014, **19**, 1530–1546.
- 4 S. Ahadian, J. Finbloom, M. Mofidfar, S. Diltemiz, F. Nasrollahi, E. Davoodi, V. Hosseini, I. Mylonaki, S. Sangabathuni, H. Montazerian, K. Fetah, R. Nasiri, M. Dokmeci, M. Stevens, T. Desai and A. Khademhosseini, Micro and nanoscale technologies in oral drug delivery, *Adv. Drug Deliv. Rev.*, 2020, **157**, 37–62.
- 5 D. McMahon and B. Oommen, in *Advanced Dairy Chemistry: Volume 1A: Proteins: Basic Aspects, 4th Edition*, eds. P. L. H. McSweeney and P. F. Fox, Springer US, Boston, MA, 2013, 185–209.
- 6 N. Lima, F. Casanova, S. Nogueira, d. C. Novaes, J. de Sa Peixoto, R. Teixeira, P. Stringheta and A. de Carvalho, Use of a crosslinked casein micelle hydrogel as a carrier for jaboticaba (*Myrciaria cauliflora*) extract, *Food Hydrocoll.*, 2020, **106**, 105872.
- 7 C. Liu, M. Li, J. Yang, L. Xiong and Q. Sun, Fabrication and characterization of biocompatible hybrid nanoparticles from spontaneous co-assembly of casein/gliadin and proanthocyanidin, *Food Hydrocoll.*, 2017, **73**, 74–89.
- 8 Y. Luo, K. Pan and Q. Zhong, Casein/pectin nanocomplexes as potential oral delivery vehicles, *International J. Pharm.*, 2015, **486**, 59–68.
- 9 S. Tan, A. Ebrahimi and T. Langrish, Controlled release of caffeine from tablets of spray-dried casein gels, *Food Hydrocoll.*, 2019, **88**, 13–20.
- 10 B. Yan, S. Davachi, R. Ravanfar, Y. Dadmohammadi, T. Deisenroth, T. Pho, P. Odorisio, R. Darji and A. Abbaspourrad, Improvement of vitamin C stability in vitamin gummies by encapsulation in casein gel, *Food Hydrocoll.*, 2021, **113**, 106414.
- 11 J. Lucey, in *Cheese: Chemistry, Physics and Microbiology, Vol 1-2, 4th Edition*, eds. P. L. H. McSweeney, P. F. Fox, P. D. Cotter and D. W. Everett, Academic Press, New York, NY, 2017, 179–197.
- 12 G. Miranda and J. Pelissier, Kinetic studies of in vivo digestion of bovine unheated skim-milk proteins in the rat stomach, *J. Dairy Res.*, 1983, **50**, 27–36.
- 13 T. Huppertz and L. Chia, Milk protein coagulation under gastric conditions: A review, *Int. Dairy J.*, 2021, **113**, 104882.
- 14 T. France, A. Kelly, S. Crowley and J. O'Mahony, The effects of temperature and transmembrane pressure on protein, calcium and plasmin partitioning during microfiltration of skim milk, *Int. Dairy J.*, 2021, **114**, 104930.
- 15 S. Gaber, A. Johansen, R. Schüller, T. Devold, E. Rukke and S. Skeie, Effect of freezing temperatures and time on mineral balance, particle size, rennet and acid coagulation of casein concentrates produced by microfiltration, *Int. Dairy J.*, 2020, **101**, 104563.
- 16 S. Schiffer, B. Adekunle, A. Matyssek, M. Hartinger and U. Kulozik, Effect of pre-heating prior to low temperature 0.1 µm-microfiltration of milk on casein-whey protein fractionation, *Foods*, 2021, **10**, 1090.
- 17 J. Ren, M. Liao, L. Ma, F. Chen, X. Liao, X. Hu, S. Miao, J. Fitzpatrick and J. Ji, Effect of spray freeze drying on the structural modification and rehydration characteristics of micellar casein powders, *Innov. Food Sci. Emerg. Technol.*, 2022, **80**, 103093.
- 18 P. John and C. Steven, The functions and roles of the Extracellular Ca²⁺-Sensing Receptor along the gastrointestinal tract, *Annu. Rev. Physiol.*, 2009, **71**, 205–217.
- 19 L. Kalantzi, K. Goumas, V. Kalioras, B. Abrahamsson, J. Dressman and C. Reppas, Characterization of the human upper gastrointestinal contents under conditions simulating bioavailability/bioequivalence studies, *Pharm. Res.*, 2006, **23**, 165–176.
- 20 Y. Shen, N. Zhang, J. Tian, G. Xin, L. Liu, X. Sun and B. Li, Advanced approaches for improving bioavailability and controlled release of anthocyanins, *J. Control. Release*, 2022, **341**, 285–299.
- 21 H. Wu, G. Oliveira and M. Lila, Protein-binding approaches for improving bioaccessibility and bioavailability of anthocyanins, *Compr. Rev. Food Sci. Food Saf.*, 2023, **22**, 333–354.
- 22 H. Gui, L. Sun, R. Liu, X. Si, D. Li, Y. Wang, C. Shu, X. Sun, Q. Jiang, Y. Qiao, B. Li and J. Tian, Current knowledge of anthocyanin metabolism in the digestive tract: absorption, distribution, degradation, and interconversion, *Crit Rev Food Sci Nutr*, 2022, 1–14.
- 23 A. Rashwan, N. Karim, Y. Xu, J. Xie, H. Cui, M. Mozafari and W. Chen, Potential micro-/nano-encapsulation systems for improving stability and bioavailability of anthocyanins: An updated review, *Crit. Rev. Food Sci. Nutr.*, 2021, 1–24.
- 24 F. Lu, Y. Zhang, C. Ma and X. Wang, Simulation and experimental study on the evolution of droplet size distribution during spray drying of mannitol, *Chem. Ind. Eng. Prog.*, 2019, **38**, 772–778.
- 25 Z. Huang, K. Li, L. Ma, F. Chen, X. Liao, X. Hu and J. Ji, Flavor release from lactose/protein matrix during storage: Effects of lactose crystallization and powder microstructure, *LWT - Food Sci. Technol.*, 2021, **141**, 110857.
- 26 M. Liao, L. Ma, S. Miao, X. Hu, X. Liao, F. Chen and J. Ji, The in-vitro digestion behaviors of milk proteins acting as wall materials in spray-dried microparticles: Effects on the release of loaded blueberry anthocyanins, *Food Hydrocoll.*, 2021, **115**, 106620.
- 27 A. Brodkorb, L. Egger, M. Alminger, P. Alvito, R. Assuncao, S. Ballance, T. Bohn, L. Bourlieu, R. Boutrou, F. Carriere, A. Clemente, M. Corredig, D. Dupont, C. Dufour, C. Edwards, M. Golding, S. Karakaya, B. Kirkhus, S. Le Feunteun, U. Lesmes, A. Macierzanka, A. Mackie, C. Martins, S. Marze, D. McClements, O. Menard, M. Minekus, R. Portmann, C. Santos, I. Souchon, R. Singh, G. Vegarud, M. Wickham, W. Weitschies and I. Recio, INFOGEST static in vitro simulation of gastrointestinal food digestion, *Nat. Protoc.*, 2019, **14**, 991–1014.
- 28 W. Yin, L. Song, Y. Huang, F. Chen, X. Hu, L. Ma and J. Ji, Glycated alpha-lactalbumin based micelles for quercetin delivery: Physicochemical stability and fate of simulated digestion, *Food Chem. X*, 2022, **13**, 100257.

- 29 A. Halabi, T. Croguennec, S. Bouhallab, D. Dupont and A. Deglaire, Modification of protein structures by altering the whey protein profile and heat treatment affects in vitro static digestion of model infant milk formulas, *Food Funct.*, 2020, **11**, 6933–6945.
- 30 R. Li, C. J., T. Rovers, B. Svensson, R. Ipsen, J. Kirkensgaard and B. H., In situ SAXS study of non-fat milk model systems during heat treatment and acidification, *Food Res. Int.*, 2022, **157**, 111292.
- 31 S. Yang, A. Tyler, L. Ahrné and J. Kirkensgaard, Skimmed milk structural dynamics during high hydrostatic pressure processing from in situ SAXS, *Food Res. Int.*, 2021, **147**, 110527.
- 32 J. Teixeira, Small-angle scattering by fractal systems, *J. Appl. Crystallogr.*, 1988, **21**, 781–785.
- 33 M. Liao, F. Chen, X. Hu, S. Miao, L. Ma and J. Ji, The in-vitro digestion behaviors of micellar casein acting as wall materials in spray-dried microparticles: The relationships between colloidal calcium phosphate and the release of loaded blueberry anthocyanins, *Food Chem.*, 2022, **375**, 131864.
- 34 B. Li, Y. Zhao, M. Wang, W. Guan, J. Liu, H. Zhao and C. Brennan, Microencapsulation of roselle anthocyanins with beta-cyclodextrin and proteins enhances the thermal stability of anthocyanins, *J. Food Process. Preserv.*, 2022, **46**.
- 35 R. Dong, J. Tian, Z. Huang, Q. Yu, J. Xie, B. Li, C. Li and Y. Chen, Intermolecular binding of blueberry anthocyanins with water-soluble polysaccharides: Enhancing their thermostability and antioxidant abilities, *Food Chem.*, 2023, **410**, 135375.
- 36 G. Koutina, J. Knudsen, U. Andersen and L. Skibsted, Temperature effect on calcium and phosphorus equilibria in relation to gel formation during acidification of skim milk, *Int. Dairy J.*, 2014, **36**, 65–73.
- 37 Z. Du, N. Xu, Y. Yang, G. Li, Z. Tai, N. Li and Y. Sun, Study on internal structure of casein micelles in reconstituted skim milk powder, *Int. J. Bio. Macromol.*, 2022, **224**, 437–452.
- 38 D. Horne and D. Dalgleish, Electrostatic interaction and the kinetics of protein aggregation: α 1-casein, *Int. J. Bio. Macromol.*, 1980, **2**, 154–160.
- 39 A. Pierre and G. Brule, Mineral and protein equilibria between the colloidal and soluble phases of milk at low temperature, *J. Dairy Res.*, 1981, **48**, 417–428.
- 40 A. Post, B. Arnold, J. Weiss and J. Hinrichs, Effect of temperature and pH on the solubility of caseins: Environmental influences on the dissociation of alpha(S)- and beta-casein, *J. Dairy Sci.*, 2012, **95**, 1603–1616.
- 41 Z. Yin, Y. Wu, Y. Chen, X. Qie, M. Zeng, Z. Wang, F. Qin, J. Chen and Z. He, Analysis of the interaction between cyanidin-3-O-glucoside and casein hydrolysates and its effect on the antioxidant ability of the complexes, *Food Chem.*, 2021, **340**, 127915.
- 42 B. Miralles, J. Sanchon, R. Sanchez, M. Martinez, Y. Le Gouar, D. Dupont, L. Amigo and I. Recio, Digestion of micellar casein in duodenum cannulated pigs. Correlation between in vitro simulated gastric digestion and in vivo data, *Food Chem.*, 2021, **343**, 128424.
- 43 L. Day, J. Raynes, A. Leis, L. Liu and R. Williams, Probing the internal and external micelle structures of differently sized casein micelles from individual cows milk by dynamic light and small-angle X-ray scattering, *Food Hydrocoll.*, 2017, **69**, 150–163.
- 44 B. Ingham, A. Smialowska, G. Erlangga, M. Matia, N. Kirby, C. Wang, R. Haverkamp and A. Carr, Revisiting the interpretation of casein micelle SAXS data, *Soft Matter*, 2016, **12**, 6937–6953.
- 45 Z. Yang, Q. Gu, W. Banjar, N. Li and Y. Hemar, In situ study of skim milk structure changes under high hydrostatic pressure using synchrotron SAXS, *Food Hydrocoll.*, 2018, **77**, 772–776.
- 46 A. Bouchoux, G. Gésan, J. Pérez and B. Cabane, How to squeeze a sponge: Casein micelles under osmotic stress, a SAXS study, *Biophys. J.*, 2010, **99**, 3754–3762.
- 47 C. de Kruif, T. Huppertz, V. Urban and A. Petukhov, Casein micelles and their internal structure, *Adv. Colloid Interface Sci.*, 2012, **171–172**, 36–52.
- 48 G. Smith, E. Brok, M. Christiansen and L. Ahrné, Casein micelles in milk as sticky spheres, *Soft Matter*, 2020, **16**, 9955–9963.
- 49 F. Lazzaro, A. Bouchoux, J. Raynes, R. Williams, L. Ong, E. Hanssen, V. Lechevalier, S. Pezennec, H. Cho, A. Logan, S. Gras and F. Gaucheron, Tailoring the structure of casein micelles through a multifactorial approach to manipulate rennet coagulation properties, *Food Hydrocoll.*, 2020, **101**, 105414.
- 50 D. Dupont, M. Alric, D. Blanquet, G. Bornhorst, C. Cueva, A. Deglaire, S. Denis, M. Ferrua, R. Havenaar, J. Lelieveld, A. Mackie, M. Marzorati, O. Menard, M. Minekus, B. Miralles, I. Recio and P. Van den Abbeele, Can dynamic in vitro digestion systems mimic the physiological reality?, *Crit. Rev. Food Sci. Nutr.*, 2019, **59**, 1546–1562.